Title:

A modified subloading Cam-clay model for granular soils subjected to suffusion

Author 1:
Wang, Gang
Researcher, Department of Civil Engineering, Central South University, Changsha, China
(Formerly, Department of Civil and Environmental Engineering, Tokyo Institute of Technology, Tokyo, Japan)
wanggang123@csu.edu.cn

Author 2:
Akihiro Takahashi
Professor, Department of Civil and Environmental Engineering, Tokyo Institute of Technology, Tokyo, Japan

Full contact details of the corresponding author.
Akihiro Takahashi (Author 2)
2-12-1-M1-3 Oh-okayama, Meguro, Tokyo 152-8552, Japan
Tel: 03-5734-2593, E-mail: takahashi.a.al@m.titech.ac.jp

Geomechanics and Geoengineering, Vol. 17, No. 4, 1294-1308, 2022
Original URL:
https://doi.org/10.1080/17486025.2021.1928769

Abstract

Suffusion, one of the modes of internal erosion, occurs when fine particles are detached under hydraulic force. More fine particles are washed out with the void growth, which subsequently causes the failure of earthworks. At present, constitutive models considering suffusion are mostly established through DEM simulations and constitutive models that can capture the main features of eroded soils are quite limited. This study aims to establish constitutive equations to model the mechanical behaviour of soils subjected to suffusion by using drained triaxial experimental data. The modified subloading Cam-clay model incorporated with the normal yield surface for the eroded soil is proposed, which can express the variation of the normal yield surface with the loss of fine particles. The determination method of the erosion-related model parameters is also proposed. The erosion-related model parameters are estimated through empirical equations with curve-fitted parameters. Finally, the capability of this modified model is demonstrated through the comparisons with experimental results.

Keywords: suffusion; modified subloading Cam-clay model; constitutive equation; triaxial test

1. Introduction

Internal erosion happens when fine particles migrate through the soil skeleton under seepage flow. This phenomenon includes concentrated leak erosion, backward erosion, contact erosion, and suffusion. Sometimes the suffusion is subdivided into suffosion and suffusion (Fannin and Slangen, 2014). Internal erosion has been considered as the main reason for the collapse of dams, levees and slopes in the last three decades, which is an essential topic in the field of geotechnical engineering. A rapid slope failure with a maximum depth of 7 m and a maximum length of 50m occurred in northern Italy due to seepage erosion (Crosta and Prisco, 1999). Through the statistics of more than 10,000 dams, Foster and Spannagle (2000) found that the piping accounted for most of the large dam failures. The continuing erosion by subsurface flow could also result in levee and dam failures (Wilson et al., 2018). In this study, the term erosion is used as the suffusion type of internal erosion (without distinction to suffosion).

Experimental investigations through triaxial compression on the stress-strain behaviour of the soils subjected to erosion have been studied by many researchers (Ke and Takahashi, 2014, 2015; Ouyang and Takahashi, 2015; Chen et al., 2016; Li et al., 2017; Mehdizadeh et al., 2017 among the others). The constitutive models with reasonable accuracy, which can express the strength and deformation characteristics of eroded soils, are required to assess the long-term performance of geotechnical structures considering the erosion-induced deterioration. Present constitutive models for the eroded soils can be classified into the following two categories:

The modified constitutive models, in which the assumptions are introduced based on the observation in DEM simulations, have been developed. Muir Wood et al. (2010) simulated the particle removal process and subsequent triaxial compression tests through the DEM simulations, from which the link between the critical state line and the erosion-induced grading variation was established. By incorporating this link into the Severn-Trent model, they proposed the modified model to predict the response of eroded soils. Hicher (2013) proposed the microstructural model to simulate the effect of erosion on the mechanical behaviour of the soils. The variation of the post-erosion void ratio was incorporated into the change of the inter-particle friction angle and the contact number of the per unit volume. It was found that the erosion-induced deformations were large for the high stress ratios, which was also validated by the DEM simulations. Four erosion-induced effects were put forward, and quantitative relationships between four effects and the loss of fine particles were established through the DEM simulations (Wang et al., 2015). Both strength and deformation responses simulated by the new elastoplastic constitutive model along with four effects were in good agreement with the DEM simulations. This type of model is established based on the DEM simulations, at the same time, they are also validated by the DEM results. Therefore, the experimental results are needed to both investigate the model parameters and validate the proposed constitutive models.

The constitutive models, in which relationships between model parameters and the post-erosion state of soil are obtained through the calibration of the model using laboratory tests, can be utilised to predict the mechanical behaviour of eroded soils. Zhang and Chen (2017) developed the expressions describing relationships between the loss of fine particles and the parameters in the Duncan-Chang model. Based on a series of triaxial tests, Wang et al. (2020) found the evolution laws of the key parameters in the subloading Cam-clay model along with different fines contents. The erosion may cause variations of many model parameters, which increases the difficulty in the calibration.

Recently, by selecting the porosity as the state parameter, the constitutive model to predict the mechanical behaviour of eroded soils was proposed (Rousseau et al., 2018, 2020). The erosion-induced porosity change was regarded as the irreversible strain, which was linked to the change in the size of the yield surface. The model incorporated with the change of the critical state line to capture the hydro-mechanical behaviour of the eroded soils was also proposed (Yang et al., 2019, 2020). They established the relation between the critical void ratio and the fines content, which could describe the variation of the critical state line after erosion.

In this study, the modified subloading Cam-clay model incorporated with the normal yield surface for the eroded soils is proposed. In the following sections, we initially examine the change in the mechanical behaviour of granular material subjected to internal erosion by using laboratory experiments, which can provide constructive inspirations for the modification of the constitutive model. The development of the normal yield surface for the eroded soils is presented in detail, followed by an explanation of the determination method of the erosion-related model parameters. Finally, the capability of this model is examined by comparison with the drained triaxial compression tests.

2. Mechanical behaviour of granular soils subjected to internal erosion

In order to investigate the development of erosion and the change in the mechanical behaviour more conveniently, many research groups have developed the apparatuses (Chang and Zhang, 2011; Ke and Takahashi, 2014; Li et al., 2017). These apparatuses adopt different methods to realise the erosion by hydraulic gradient control, inflow rate control and seepage water volume control.

However, to investigate the mechanical changes caused by erosion, some researchers also try to mimic an eroded sample by making a loose sample with less fines content (Ouyang and Takahashi, 2015; Andrianatrehina et al., 2016; Hu et al., 2018). The effects of the preparing methods (preparing loose samples with less fines content or obtaining eroded samples by seepage flow) of the eroded soils are seldom reported from experiments since it is very difficult to prepare a loose sample with less fines content. These two erosion scenarios can be simulated through DEM, in which the eroded specimens prepared with different fines contents can be obtained from the random deletion of fine particles while the eroded soils by seepage flow are realised through the deletion of fine particles with the smaller contact forces (Hosn et al., 2016; Zhang et al., 2019).

Figure 1 briefly shows the apparatus assembly of the seepage tests with seepage water volume control. In the beginning, downward flow is applied to the specimen with increasing inflow water. Note that the flow rate of the seeping water should increase gradually and reach a certain value where enough fine particles can be washed out (Richards and Reddy, 2010). Afterwards, the seepage tests are terminated when the volume of inflow water reaches the designated value. Finally, the mass of the eroded fine particles dropping into the collection tank is measured to determine the post-erosion fines content. The continuing loss of fine particles makes the specimen a more open structure (Wang et al., 2020). Different parts (bottom, middle, and top) of the specimens are expected to have different fines contents or open void spaces after internal erosion (Hunter and Bowman, 2018). In the scope of the present study, the fines content denotes the mass ratio of remaining fine particles to the whole soils, which ignores the inhomogeneity of the loss of fine particles in different locations.

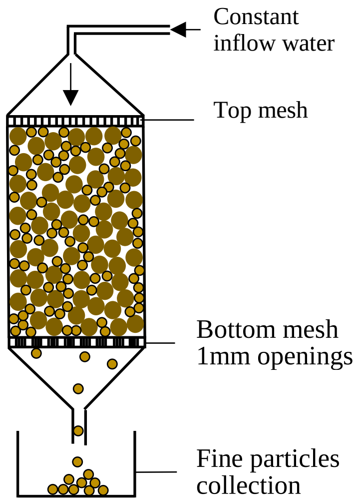

Fig. 1 Schematic diagram of downward seepage test

After the seepage tests, the drained triaxial compression tests are performed on the eroded specimens. The mechanical responses of the eroded specimen are possibly affected by the rearrangement of the particles and the heterogeneous nature of the fines' migration path (Nguyen et al., 2019). Erosion may cause a decrease in both the peak shear strength and the deviatoric stress at the critical state for the dense soils (Chen et al., 2016; Li et al., 2017, 2020) The dense soils become less dilative or more contractive with the loss of fine particles. The erosion process changes the soil from a dense state to a loose state; hence, it is expected to make the dense soil more contractive and decrease the peak strength (Muir Wood et al., 2010). However, the volumetric strain of the loose soils decreases slightly after erosion (Ke and Takahashi, 2015). The volumetric strain is defined as the volume change divided by the initial total volume ($\varepsilon_v = \Delta V/V_0 = \Delta V/(1+e_{bs})$). The volumetric strain is affected by two factors, volume change (ΔV) and the void ratio before shearing (e_{bs} includes the initial void ratio of the uneroded soils after consolidation and the post-erosion void ratio of the erode soils). The ΔV of the eroded soils during triaxial compression is larger than that of the uneroded soils during triaxial compression. At the same times, the e_{bs} also increases after erosion. When the effect of the void ratio increment is larger than that of the volume change, the volumetric strain of the internally eroded soils becomes less than that of the uneroded soils.

3. Model description

The subloading surface, geometrically similar to the normal yield surface, was proposed by Hashiguchi (1989). This subloading surface, inside the normal yield surface, always passes through the current stress state point. This indicates that the plastic deformation occurs even if the current stress state point is inside the normal yield surface, realising the smooth of stress-strain behaviour under loading. Considering the influence of temperature change on the mechanical behaviour of granular materials, the subloading Cam-clay model was modified by introducing the concept of the equivalent stress by Zhang et al. (2012). The subloading surface was also modified to model the mechanical behaviour of cement-treated soils (Gai and Sánchez, 2019). The increased amount of cement is a process that strengthens the soils. The erosion has the opposite effect, i.e., the deviatoric stress decreases after the erosion for both loose and dense soils under the drained triaxial compression condition. The volumetric strain of eroded loose soils decreases while the eroded dense soils become less dilative or become contractive after erosion. The normal yield surface of the eroded soils varies after the internal erosion. The following modified subloading Cam-clay model is inspired by the modified model for the cement-treated soils by Gai and Sánchez (2019).

3.1 Modified yield surface

The normal yield surface of the loose soils expands after erosion, which indicates that the structure (particle rearrangement) of the loose soils is reinforced after the seepage tests, but this kind of reinforcement is weak and easy to collapse (Wang et al., 2020). However, the erosion could cause the shrinkage of the normal yield surface for the dense soils as the deviatoric stress decreases and the volumetric strain becomes contractive after erosion. The concept of normal yield surface for the eroded soils is shown in Fig. 2.

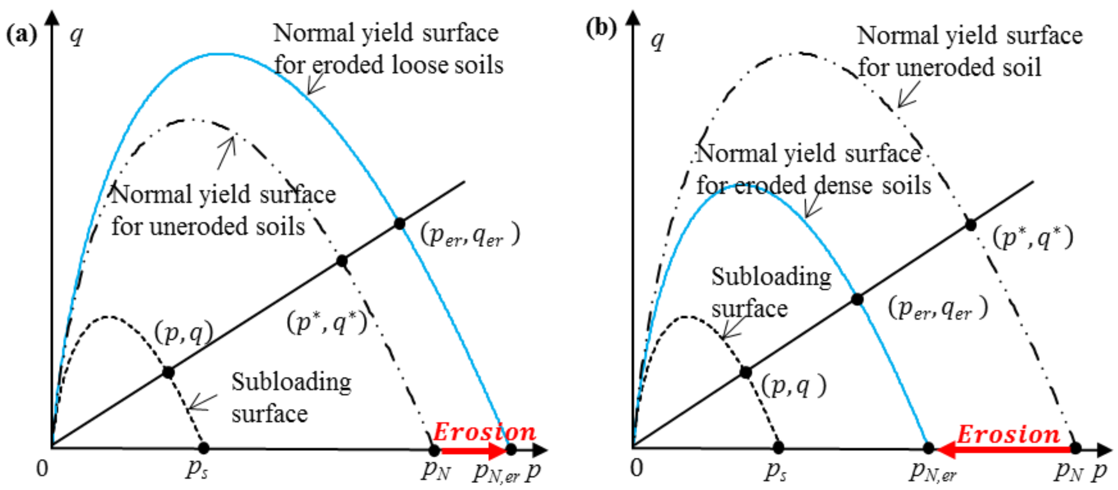

Fig. 2 Concept of normal yield surface for eroded soils. **a** loose soils, **b** dense soils

Based on the geometrical relations between different yield surfaces, we can obtain:

$$\frac{p}{p_S} = \frac{p_{er}}{p_{N,er}} = \frac{p^*}{p_N} \tag{1}$$

$$\frac{q}{p} = \frac{q_{er}}{p_{er}} = \frac{q^*}{p^*} \tag{2}$$

where (p, q) represents the current stress state; (p_{er}, q_{er}) is the stress state point on the normal yield surface for the eroded soil; (p^*, q^*) is the state point on the normal yield surface for the uneroded soil. p_s, $p_{N,er}$, p_N are the intersections of subloading yield surface, normal yield surface for the eroded soils, normal yield surface for the uneroded soils with the mean effective stress axis, respectively (all stresses in this study are effective stresses).

The normal yield surface for the eroded soils is expressed as:

$$f = C_p \ln \frac{p_{er}}{p_{N,er}} + D\frac{q_{er}}{p_{er}} = 0 \tag{3}$$

where $C_p = \frac{\lambda-\kappa}{1+e_0} = D \cdot M$ (Zhang et al., 2012), λ is the slope of the normal compression line, κ is the slope of the swelling line, e_0 is the void ratio for reference state, *M* is the critical stress ratio, *D* is the material constant (Shibata, 1963).

Similarity ratio R, 0 < $R \leq 1$, is the size ratio of the subloading yield surface to the normal yield surface of uneroded soils, which is also the reciprocal of the over-consolidation ratio (Nakai and Hinokio, 2004):

$$R = \frac{p}{p^*} = \frac{q}{q^*} = \frac{p_S}{p_N} \tag{4}$$

Similarity ratio of the eroded soils R_{er}, is the size ratio of the normal yield surface for the eroded soils to the normal yield surface for the uneroded soils:

$$R_{er} = \frac{p_{er}}{p^*} = \frac{q_{er}}{q^*} = \frac{p_{N,er}}{p_N} \tag{5}$$

For eroded loose soils, $R_{er} \geq 1$. When R_{er} decreases, the effect of erosion-induced reinforcement diminishes. When the effect of the erosion does not exist, R_{er} equals to one. For eroded dense soils, $R \leq R_{er} \leq 1$.

The normal yield surface for the eroded soils can be written as below:

$$f = C_p \ln\left(\frac{p_{er}}{p_0} \cdot \frac{p_0}{p_{N,er}}\right) + D\frac{q_{er}}{p_{er}} = 0 \tag{6}$$

where p_0 is the atmospheric pressure or the reference pressure, taken as 101 kPa in this study (Wang and Li, 2015).

Here, we assume that the plastic volumetric strain induced by the stress changing from p_0 to $p_{N,er}$ is expressed as (Zhang et al., 2012):

$$\varepsilon_v^p = C_p \ln\frac{p_{N,er}}{p_0} \tag{7}$$

Equation (6) can be written as:

$$f = C_p \ln\frac{p_{er}}{p_0} - \varepsilon_v^p + D\frac{q_{er}}{p_{er}} = 0 \tag{8}$$

This equation can be rearranged in the form of the current stress state (p, q) as below:

$$f = C_p \ln\left(\frac{p}{p_0} \cdot \frac{p_{er}}{p^*} \cdot \frac{p^*}{p}\right) - \varepsilon_v^p + D\frac{q}{p} = 0 \tag{9}$$

Substituting Eqns. (4) and (5) into Eqn. (9), we can obtain the following equation for the subloading surface:

$$f = C_p \ln\frac{p}{p_0} + C_p \ln R_{er} - C_p \ln R - \varepsilon_v^p + D\frac{q}{p} = 0 \tag{10}$$

3.2 Plastic potential, flow rule and consistency condition

The associated flow rule is applied to the subloading surface. The plastic volumetric strain increment and plastic shear strain increment can be obtained from the following equations:

$$d\varepsilon_v^p = \Lambda\frac{\partial f}{\partial p} \tag{11}$$

$$d\varepsilon_q^p = \Lambda\frac{\partial f}{\partial q} \tag{12}$$

in which Λ is the plastic multiplier.

The hardening law of R is expressed as:

$$dR = -\frac{m_R}{D}\ln R \cdot d\varepsilon_q^p \tag{13}$$

where m_R is a material constant, determined by the degrading rate of the over-consolidation.

The construction of the evolution law of R_{er} considers that the increment of R_{er} is related to the plastic shear strain. Then the evolution law of R_{er} is expressed as:

$$dR_{er} = h_0 \cdot \left(\frac{1}{R_{er}} - 1\right) \cdot d\varepsilon_q^p \tag{14}$$

where h_0 is a material constant, which is determined by the degrading rate of the effect caused by erosion.

Since the current stress state remains on the subloading surface during the plastic flow, the consistency equation is applied to the subloading surface of the eroded soils, as shown in Eqn. (15):

$$df = \frac{\partial f}{\partial p}dp + \frac{\partial f}{\partial q}dq + \frac{\partial f}{\partial R}dR + \frac{\partial f}{\partial \varepsilon_v^p}d\varepsilon_v^p + \frac{\partial f}{\partial R_{er}}dR_{er} = 0 \tag{15}$$

The plastic multiplier can be obtained as:

$$\Lambda = \frac{\frac{\partial f}{\partial p} \cdot K \cdot d\varepsilon_v + \frac{\partial f}{\partial q} \cdot 3G \cdot d\varepsilon_q}{K \cdot \left(\frac{\partial f}{\partial p}\right)^2 + 3G \cdot \left(\frac{\partial f}{\partial q}\right)^2 + H} \tag{16}$$

where *K* is the bulk modulus and *G* is the shear modulus. *K* and *G* can be obtained from the equations below (Richart et al., 1970):

$$G = G_0 \frac{(2.97 - e)^2}{1 + e} \sqrt{p p_0} \tag{17}$$

$$K = G \frac{2(1 + v)}{3(1 - 2v)} \tag{18}$$

where G_0 is the material constant, *e* is the void ratio, *v* is the Poisson's ratio.

H is the hardening function and is expressed as:

$$H = -\frac{\partial f}{\partial \boldsymbol{k}} \cdot \frac{\partial \boldsymbol{k}^T}{\partial \varepsilon_{ij}^p} \cdot \frac{\partial f}{\partial \sigma_{ij}} \tag{19}$$

where *T* denotes the transpose, ***k*** indicates the hardening parameters in this study, ε_v^p, *R* and R_{er} respectively.

3.3 Stress-strain relationship

The elastoplastic equation with the triaxial stress and strain parameters is expressed as:

$$\begin{pmatrix} dp \\ dq \end{pmatrix} = \boldsymbol{D}_{ep} \begin{pmatrix} d\varepsilon_v \\ d\varepsilon_q \end{pmatrix} \tag{20}$$

where $\boldsymbol{D_{ep}}$ is the elastoplastic stiffness matrix, $\boldsymbol{D}_{ep} = \boldsymbol{D}_e - \frac{\boldsymbol{D}_e \partial \boldsymbol{f} \partial \boldsymbol{f}^T \boldsymbol{D}_e}{\partial \boldsymbol{f}^T \boldsymbol{D}_e \partial \boldsymbol{f} + H}$, in which $\boldsymbol{D}_e = \begin{bmatrix} K & 0 \\ 0 & 3G \end{bmatrix}$, and $\partial \boldsymbol{f}^T = \begin{Bmatrix} \frac{\partial f}{\partial p} & \frac{\partial f}{\partial q} \end{Bmatrix}$.

4. Effects of erosion on model parameters

Ke and Takahashi (2014) performed a series of seepage tests under different conditions: initial fines content 35% under varied confining pressures (50, 100 and 200 kPa); the same confining pressure (50 kPa) with different initial fines contents (15%, 25% and 35%). These specimens were loose sands. Chen et al. (2016) investigated the variations of the material properties of the dense sands subjected to seepage flow. The table salt functioned as a part of fine particles was added into the soils during the sample preparation, and then was dissolved into the water under the 50 kPa confining pressure. Although the loss of fine particles mimicked by the dissolution of the table salt is not exactly the same as that by seepage flow, at least, we can study the effects of the loss of fine particles through their experiments and the similar technique, i.e., the removal of particles, has been used in the numerical studies as well (Muir Wood et al., 2010; Hicher, 2013). Two groups of dense sands were studied: Group A, the soils with 20% initial fines content have cumulative fines losses 0%, 5% and 15% after the salt dissolution; Group B, the soils with 35% initial fines content have cumulative fines losses 0%, 10% and 30% after the salt dissolution. Li et al. (2020) also studied the mechanical behaviour of the dense soils under 50 kPa confining pressure with 32% initial fines content, the cumulative fines losses are 0%, 4.1% and 10.2% after erosion. The material composition and physical properties are summarised in Table 1. The modified model is used to simulate the mechanical behaviour of these eroded soils (Figs. 3, 4, and 5). The modified model can capture the main features of both uneroded and eroded soils under different confining pressures and different cumulative fines losses.

The model parameters are summarised in Table 2. e_c denotes the initial void ratio after consolidation, which can be obtained after the consolidation of the specimen; ΔFC represents the cumulative fines content, the mass ratio of the eroded fines to the initial total soils, which can be obtained after the seepage tests. λ and κ are normally obtained from the isotropic compression tests, and it is reasonable to obtain them from the back analysis of the shearing behaviour of the uneroded and eroded soils. M can be obtained from the deviatoric stress at the critical state of both uneroded and eroded soils. G_0, R_0, v, m_R, h_0 can be obtained from the back analysis on the uneroded soils, and are assumed to be unchanged for eroded soils for simplification. $R_{er,0}$ is obtained from a back analysis of the mechanical behaviour of both eroded and uneroded soils under the drained triaxial compression condition. These parameters will be further discussed in the following sections.

Table 1 Materials and physical properties of soils subjected to internal erosion

Case	Coarse	Fines	FC_0	C_u	C_c	References
1	Silica No.3	Silica No.8	15%	13	7.9	Ke and Takahashi (2014)
2	Silica No.3	Silica No.8	25%	17	7.9	Ke and Takahashi (2014)
3	Silica No.3	Silica No.8	35%	18	0.25	Ke and Takahashi (2014)
4	Completely decomposed granite	Leighton Buzzard sand	20%	-	-	Group A, Chen et al. (2016)
5	Completely decomposed granite	Leighton Buzzard sand	35%	16.7	0.09	Group B, Chen et al. (2016)
6	10mm Basalt	Silica 60G, 5mm Basalt	32%	284.6	5.6	Li et al. (2020)

Note: FC_0 denotes the initial fines content; C_u represents the uniformity coefficient; C_c represents the curvature coefficient; "-" indicates that the information is not given.

Table 2 Model parameters used in modified model

Samples	e_c	ΔFC	λ	κ	M	G_0	v	R_0	m_R	$R_{er,0}$	h_0	References
50E35	0.55	29.3%	0.072	0.014	1.47	100	0.2	0.71	0.2	1.17	100	Ke and Takahashi (2014)
100E35	0.56	23.0%	0.069	0.014	1.51	100	0.2	1	0.2	1.11	100	
200E35	0.54	13.8%	0.064	0.014	1.53	100	0.2	1	0.2	1.06	100	
50E35	0.38	0%	0.045	0.01	1.45	100	0.3	0.125	0.3	1	100	Group B soils, Chen et al. (2016)
50E35	0.38	10%	0.084	0.01	1.36	100	0.3	0.125	0.3	0.7	100	
50E35	0.38	30%	0.098	0.01	1.28	100	0.3	0.125	0.3	0.625	100	
50E32	0.33	0%	0.060	0.02	1.76	150	0.3	0.048	0.5	1	200	Li et al. (2020)
50E32	0.33	4.1%	0.065	0.02	1.70	150	0.3	0.048	0.5	0.85	200	
50E32	0.33	10.2%	0.068	0.02	1.65	150	0.3	0.048	0.5	0.78	200	

Note: “50E35”, where “50” indicates the confining pressure is 50kPa, “E” denotes the erosion, “35” presents that the initial fines content is 35%; ¨0.33¨, the initial void ratio for this case is not given, which is calculated based on Eqn. (22).

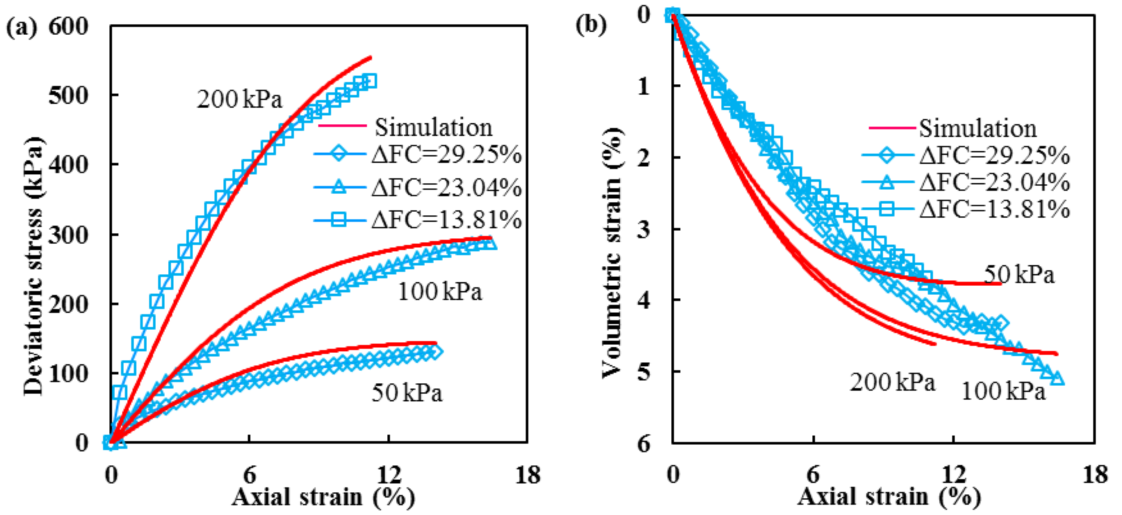

Fig. 3 Typical simulation results of drained triaxial compression after erosion through modified model on loose soils; **(a)** stress-strain response, **(b)** volumetric strain-axial strain response (After Ke and Takahashi, 2014)

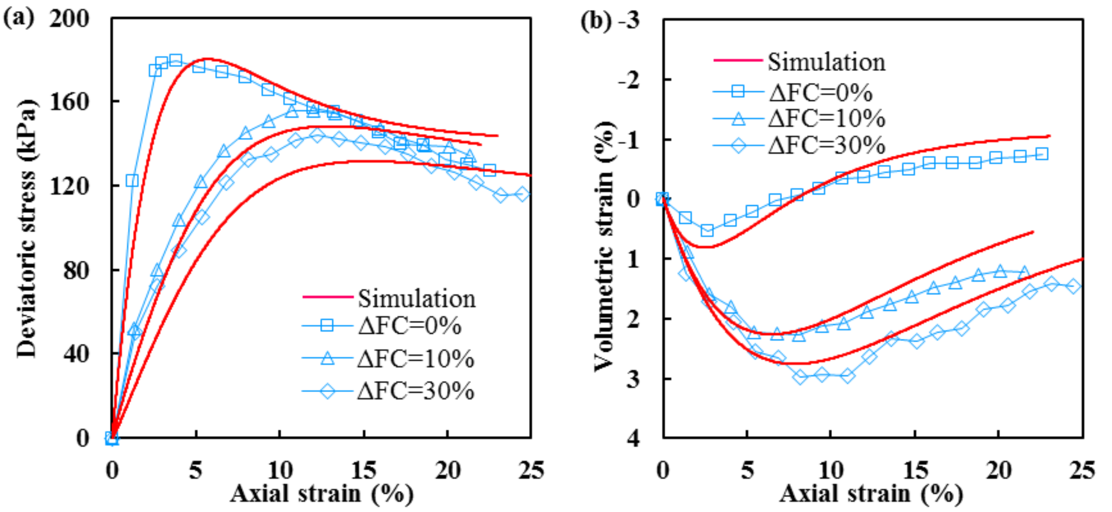

Fig. 4 Simulation results of drained triaxial compression tests after erosion through modified model on dense soils (Group B); **(a)** stress-strain response, **(b)** volumetric strain-axial strain response (After Chen et al., 2016)

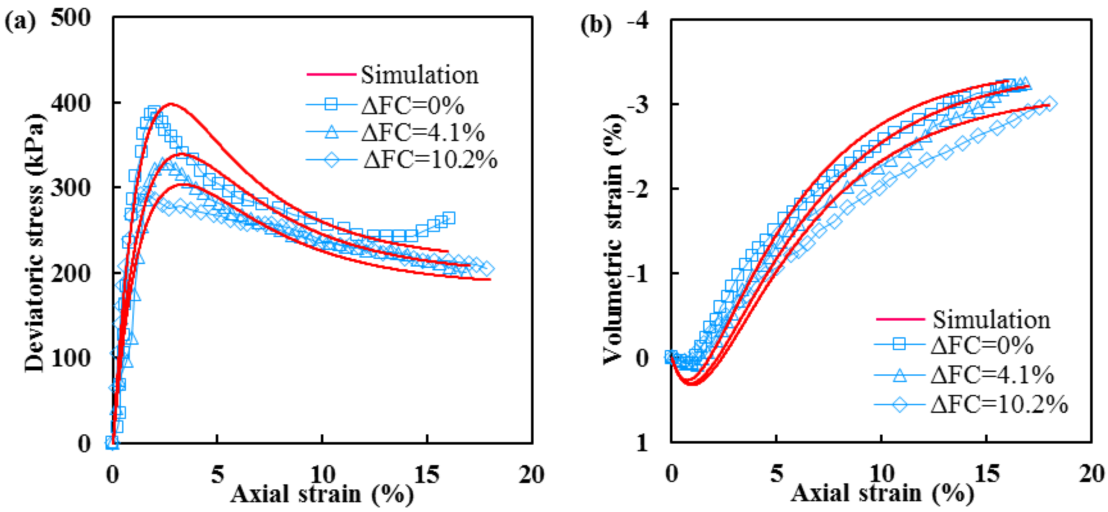

Fig. 5 Simulation results of drained triaxial compression tests after erosion through the modified model on dense soils. **a** stress-strain response, **b** volumetric strain-axial strain response (After Li et al., 2020)

4.1 Change in void ratio after erosion

The erosion could cause the loss of fine particles, resulting in an increase in the void ratio (Ke and Takahashi, 2014; Hu et al., 2020). The erosion-induced change in volume was found in some experiments (Xiao and Shwiyhat, 2012; Ke and Takahashi, 2014). However, no volume change erosion also happens due to the seepage flow (Fannin and Slangen, 2014). The possible explanation may be that the soils are constituted by two parts: the stable skeleton (mainly coarse particles) and the migratable particles that do not contribute to the stress transmission (mainly fine particles). When the cumulative fines loss is small or the skeleton is competent enough, the volume may be unchanged even the erosion occurs due to the seepage flow, i.e., the soil is expected to show suffusion type erosion. Li et al. (2020) reported that the volumetric strain is zero when the cumulative fines loss is smaller than 4%.

Contrarily, when the cumulative fines loss is large or the skeleton collapses by the large seepage force, the volume may change dramatically but not indefinitely. Chen et al. (2017) measured the volumetric strain of eroded soils during the seepage test through the developed photographic method, which was found to be unchanged under both triaxial compression and extension conditions when the erosion ratio ranged from 80% to 100%. Zhuang et al. (2021) reported that both cumulative chemical dissolution and fine particle migration could cause the settlement of the loess: From the laboratory seepage tests, the variation of the volume change for the loess along with the elapsed time could be measured. Within the first two days, the volume did not change. The gradient of the volume change increased with the elapsed time gradually, and then decreased, finally tended to be zero. This experimental evidence supports that the maximum volumetric strain $\varepsilon_{v\max}^{er}$ may exist for the soils subjected to the seepage flow.

Estimation of the erosion-induced volumetric strain from the cumulative fines loss is useful for the modelling of eroded soil behaviour. Here, according to the experimental evidence mentioned above, it is assumed that depending on the cumulative fines loss ΔFC, the erosion-induced volumetric strain varies from zero to the maximum volumetric strain $\varepsilon_{v\max}^{er}$. This may be expressed by:

$$\varepsilon_v^{er} = \frac{1}{2}\varepsilon_{v\max}^{er}\left(1 + \tanh\left(\frac{1}{l}(\Delta FC - A)\right)\right) \tag{21}$$

where A is the threshold, l is a parameter deciding the smoothness of the fitting curve (see Fig. 6). From the fitting of the experimental data, $\varepsilon_{v\max}^{er}$, A and l are taken as 20%, 19% and 0.095 for dense sands (Group B, Chen et al., 2016); 4.2%, 16% and 0.055 for loose sands (Ke and Takahashi, 2014). The soil parameters from experiments for the uneroded and eroded soils are summarised in Table 3. The underestimation of the volumetric strain for loose sands with 35% initial fines content under 200 kPa confining pressure could be explained by the ignorance of the effect of confining pressure. From the fitting curve, we can know that the erosion-induced volumetric strain is almost zero when the cumulative fines loss is less than 5% for loose sands. When the cumulative fines loss is more than 25%, the volumetric strain of loose sands shows almost the greatest value but becomes insensitive to the amount of fines loss. The change of volumetric strain for dense sands has a similar trend.

Table 3 Soil parameters from experiments before and after seepage tests

Samples	e_c	ΔFC	e_{er}	ε_v^{er}	References
50E15	0.68	4.9%	0.78	0.01%	Ke and Takahashi (2014)
50E25	0.57	15.2%	0.81	0.8%	
50E35	0.55	29.3%	1.01	3.9%	
100E35	0.56	23.0%	0.92	3.7%	
200E35	0.54	13.8%	0.77	2.8%	
50E35	0.38	0%	0.38	0%	Group B soils, Chen et al. (2016)
50E35	0.38	10%	0.48	3.6%	
50E35	0.38	30%	0.59	19.1%	

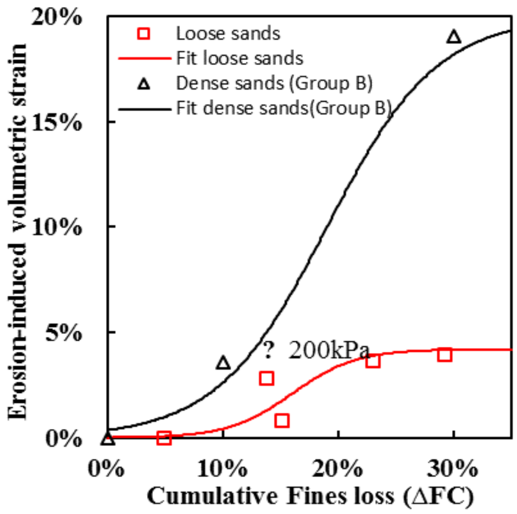

Fig. 6 Erosion-induced volumetric strain against cumulative fines loss

If we know the volumetric strain induced by erosion, we can estimate the post-erosion void ratio (Ke and Takahashi, 2014). The equation is as follow:

$$e_{er} = (1-\varepsilon_v^{er})\left(\frac{e_c + \Delta FC}{1-\Delta FC}\right) - \varepsilon_v^{er} \tag{22}$$

where ΔFC is regarded as a percentage by volume when the specific gravities of both the coarse and fine particles are the same. The post-erosion void ratios from both experiments and calculations are plotted in Fig. 7. Equation (22) can be used to estimate the post-erosion void ratios accurately by considering the cumulative fines loss and erosion-induced volumetric strain.

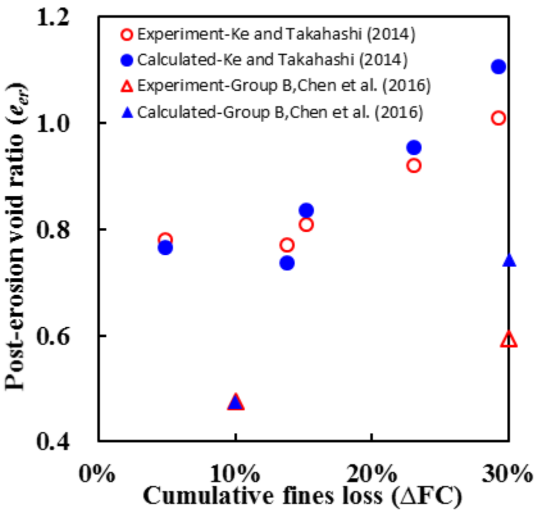

Fig. 7 Post-erosion void ratio comparison between experimental and calculated results

4.2 Initial void ratio before shearing-dependent slope of normal compression line (λ)

The compression index (= 0.434·λ) is usually obtained from the consolidation test, which is costly and timeconsuming (Habibbeygi et al., 2017). Many empirical formulations of the compression index with parameters such as liquid limit, void ratio, and water content have been proposed. The positive linear relationship between the compression index and these parameters has been obtained from various soils (Park and Koumoto, 2004; Park and Lee, 2011; Tiwari and Ajmera, 2012). The liquid limit was mostly used to estimate the compression index of the clays, reflecting the soil type and the soil surface characteristics. For sandy soils, as the normal compression line is not unique for soil and depends on the state of the soil, the void ratio could be used in such a case. Al-Khafaji and Andersland (1992) propose to use the water content for the compression index estimation.

Since (1) the internally unstable soils are typically sandy soils and (2) the compression index for such soil may depend on the state of the soil and it is expected that the larger the void ratio the more compressible the soil, the initial void ratio before shearing is selected as a variable to estimate the slope of the normal compression line of the soil mixture in this study. The relationships between the slope of the normal compression line and the void ratio before shearing for all examined soils are plotted in Fig. 8 and are fitted by:

$$\lambda(e_{bs}) = a_1 \cdot e_{bs} + b_1 \tag{23}$$

where a_1 is the gradient of the λ; b_1 is the intercept of the λ-axis; e_{bs} denotes the initial void ratio before shearing. Figure 8 indicates that the slope of the normal compression line increases with the initial void ratio before shearing for all the examined soils. Depending on the initial fines contents and the material compositions, the gradient a_1 and the intercepts b_1 are different for different examined soils.

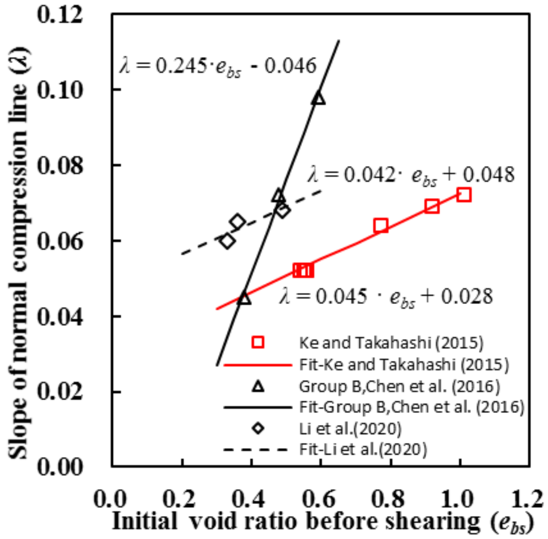

Fig. 8 Relationship between slope of normal compression line and initial void ratio before shearing

4.3 Final fines content-dependent angle of shearing resistance at critical state (φ)

The critical stress ratio (M) can be estimated from the critical strength from the stress path. The existence of fines in the sand can alter the mechanical behaviour of the sand, such as the resistance to liquefaction, the angle of shearing resistance at both peak and critical state (Seed and Lee, 1966). Previous studies showed that there exists a certain relationship between the angle of shearing resistance and fines content (Cabalar, 2011; Zuo and Baudet, 2015; Benahmed et al. 2015; Mahmoudi et al., 2018; Xiao et al., 2017). And also the empirical formulation is helpful for the calculation of the preliminary design of small projects (Wichtmann et al., 2015). Thus, such a relationship is examined for the eroded soils in this study. The relationships between the angle of shearing resistance at the critical state (φ) and final fines content (FC_∞) for both loose and dense sands are plotted in Fig. 9 and are fitted by:

$$\varphi(FC_\infty) = a_2 \cdot FC_\infty + b_2 \tag{24}$$

where a_2 is the gradient of the angle of shearing resistance at the critical state to FC_∞; b_2 is the angle of shearing resistance at the critical state for the soils when FC_∞ equals to zero. Figure 9 indicates that the angle of shearing resistance at the critical state increases with the final fines content when the final fines content is smaller than the threshold fines content. Depending on the particle shape, mineral composition, packing density, and the stress state, the gradient of the angle of the shearing resistance at critical state (a_2) and the angle of shearing resistance at critical state for the soils without fines (b_2) are different as expected.

Increasing amounts of fine particles can occupy more space formed by coarse particles, which may be not positioned with the optimum interlocking at the beginning. With the continuing shearing, fine particles rearrange and reach a more stable state, which results in the increasing interlocking and angle of shearing resistance at the critical state (Salgado et al., 2000). Carraro et al. (2009) advocated that the soil mixture with more fine particles needs more energy for the occurrence of shearing at the constant volume (critical state). Chang and Yin (2011) proposed that the increase of fine particles could increase the particles wedging, which could add to the angle of shearing resistance at the critical state. According to these previous works, it can be said that the relationships obtained are reasonable.

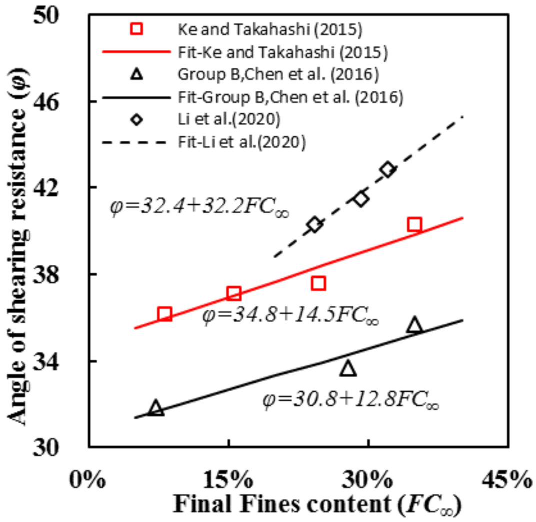

Fig. 9 Relationship between angle of shearing resistance at critical state and final fines content

4.4 Normalised cumulative fines loss-dependent initial similarity ratio ($R_{er,0}$)

The initial similarity ratio of the eroded soils ($R_{er,0}$) should be determined by the extent of the erosion prior to shearing. The initial similarity ratio $R_{er,0}$ of the eroded soils is expressed by using $\Delta p_{N,0}$ as:

$$R_{er,0} = \frac{p_{N,er0}}{p_{N,0}} = \frac{p_{N,0} + \Delta p_{N,0}}{p_{N,0}} \tag{25}$$

where $\Delta p_{N,0}$ is an initial stress parameter that represents the change in the size of the normal yield surface by erosion, $p_{N,0}$ is the initial intersection of the normal yield surface of uneroded soils and the mean effective stress axis (pre-consolidation stress). $\Delta p_{N,0}$ is assumed to be related to both the cumulative fines loss and initial fines content, expressed as:

$$\Delta p_{N,0} = \beta_0 \cdot \left(\frac{\Delta FC}{FC_0}\right)^{\alpha_0} \cdot p_{N,0} \tag{26}$$

where α_0 and β_0 are material constants. By substituting Eqn. (26) into Eqn. (25), we can get:

$$R_{er,0} = \frac{p_{N,0} + \beta_0 \cdot \left(\frac{\Delta FC}{FC}\right)^{\alpha_0} \cdot p_{N,0}}{p_{N,0}} = 1 + \beta_0 \cdot \left(\frac{\Delta FC}{FC_0}\right)^{\alpha_0} \tag{27}$$

The initial similarity ratios can be obtained from the back analysis of different series of drained triaxial tests with different cumulative fines losses. The relationships between the initial similarity ratio and normalised cumulative fines loss are plotted in Fig. 10. The initial similarity ratio for the dense soils decreases from one with the loss of fine particles, while the initial similarity ratio for the loose soils slightly increases with the loss of fine particles.

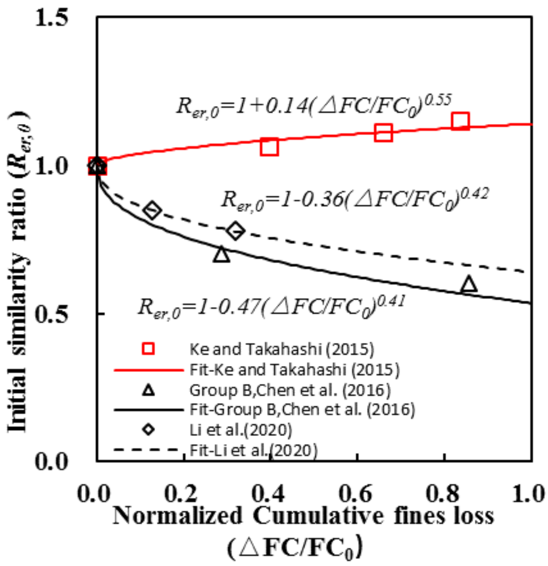

Fig. 10 Relationship between initial similarity ratio and normalised cumulative fines content

4.5 Determination of initial conditions considering internal erosion

The shear behaviour of soils is affected by the extent of internal erosion. The above-mentioned parameters, such as the erosion-induced volumetric strain, post-erosion void ratio, the angle of shearing resistance at the critical state, the slope of the normal compression line, and the initial similarity ratio of eroded soils, may have a great impact on the soil responses. Seepage tests are needed to determine the erosion parameters (erosion-induced volumetric strain and post-erosion void ratio). The number and type of seepage tests depend on many conditions (e.g., confining pressure, initial fines content, and flow velocity). When only confining pressures are different, a series of seepage tests under different confining pressures with the same initial fines contents and constant flow velocity need to be performed. However, when initial fines content and flow velocity change, more seepage tests considering the variations of initial fines content and flow velocity need to be performed. Then, a series of triaxial tests on the eroded soils need to be performed. Based on the variation of the deviatoric stress at the critical state, the variation of the shearing resistance at the critical state along with the initial void ratio before shearing can be obtained. Based on the back analysis of the experimental results, the evolution of the similarity ratio and the slope of the normal compression line along with erosion parameters can be obtained. By using the equations above, it is possible to determine the parameters needed for the calculation of the responses of the internally eroded soils, as shown in Fig. 11.

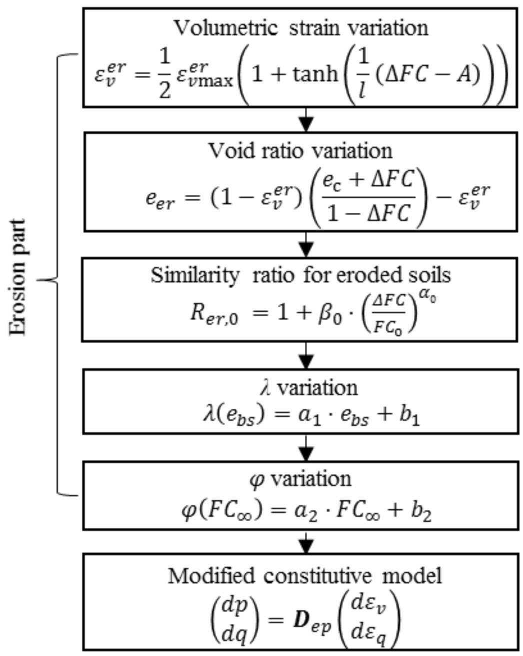

Fig. 11 Determination of parameters for calculation of responses of internally eroded soils

5. Model performance

To evaluate the predictive ability of the modified model, a series of triaxial tests with different cumulative fines losses under the same confining pressure is simulated.

5.1 Calibration of parameters

The drained triaxial compression tests (Group A) performed by Chen et al. (2016), which have not been used in the previous section, are described in the present section. The poorly graded specimen was prepared by a mixture of two types of sand having different particle sizes. The initial fines content was 20%. The drained triaxial compression tests were performed with the 50 kPa confining pressure. The parameters for the modified model can be divided into two parts: 1) the model parameters for the uneroded soil, the slopes of normal compression line and swelling line in the e-ln p space (λ and κ), which can be obtained from the isotropic compression test. M is the critical stress ratio, which can be obtained from the triaxial compression test. R_0 is the initial stress ratio, and m_R is the degradation factor of the stress ratio, which can be obtained from the back analysis of the triaxial compression tests. ν is Poisson's ratio, which is selected as 0.3. G_0 is the initial shear modulus, taken as 100 MPa. 2) the model parameters for the eroded soil, α_0 and β_0 can be obtained from the equation for Group B soil in Fig. 10. h_0 can be estimated from the value for Group B soil in Table 2. a_1 and a_2 are estimated by the calibration for the Group B soil in Figs. 8 and 9; A, l, $\varepsilon_{v\max}^{er}$ are estimated by the fitting of the erosion-induced volumetric strain against the cumulative fines loss for the dense soil in Fig. 6. All parameters are summarised in Tables 4 and 5.

Table 4 Material parameters and physical constants for soils

Case	Original Model Parameters							
	λ	κ	M	e_c	R_0	m_R	G_0	ν
Group A, Chen et al. (2016)	0.055	0.01	1.35	0.461	0.12	0.3	100	0.3

Table 5 Erosion parameters for soils

Case	Erosion Parameters							
	h_0	α_0	β_0	A	l	ε_v^{er}	a_1	a_2
Group A, Chen et al. (2016)	100	0.41	-0.47	19%	0.095	20%	0.245	12.8

5.2 Simulations of drained triaxial tests on eroded soil

Figure 12 shows the comparisons between experimental and simulation results of dense soils (Group A, Chen et al., 2016). The soils were subjected to seepage flow, after which the drained triaxial compression test was performed. The soils have the same initial void ratios 0.461 before erosion, exhibiting the dilative behaviour. The deviatoric stress increases to the peak and then decreases for all the soils. However, both peak strength and deviatoric stress at the critical state decrease for the soils with 5% and 15% cumulative fines losses. With the increase of cumulative fines loss, the volumetric strain changes from dilative to contractive.

A good agreement is obtained between the experimental and simulation results. The modified constitutive model can capture the mechanical behaviour of the eroded soils at the dense state.

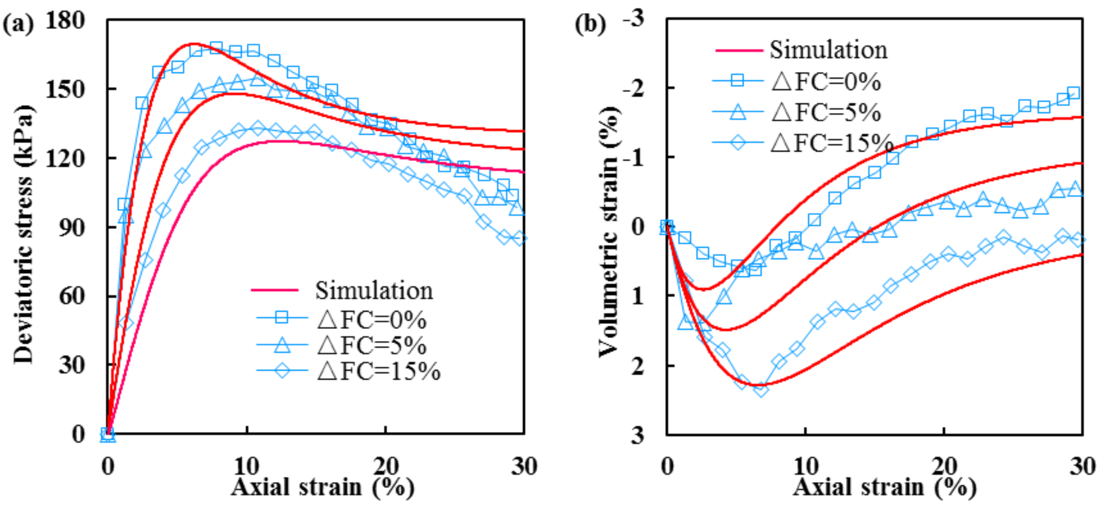

Fig. 12 Comparison between experimental and simulation results of drained triaxial compression after erosion on dense soils (Group A, Chen et al.,2016); **(a)** stress-strain response, **(b)** volumetric strain-axial strain response

5.3 Effects of degradation parameter h_0

The parameter h_0 represents the degradation of the similarity ratio (R_{er}). The soils (Group A, Chen et al., 2016) with 15% cumulative fines loss are considered to study the effect of the degradation parameter on the evolution of the similarity ratio for the eroded dense soils. Figure 13 shows the variation of the similarity ratio for the eroded dense soils under different degradation parameters h_0. The similarity ratio for the eroded dense soils increases with shearing and finally reaches one, which indicates that the effect of erosion fades with the continuing shearing. The greater the value of the degradation parameter h_0, the faster the degradation of the erosion effect.

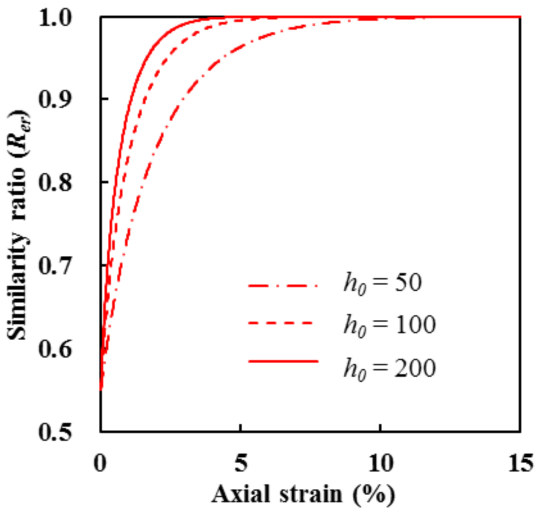

Fig. 13 Variation of similarity ratio of dense soils (R_{er}) along with axial strain under different degradation parameters

5.4 Applicability of proposed model for eroded soils

The predictive equations can be used to estimate the seepage-induced variation of some properties (e.g., fines content, volumetric strain) for the gap-graded soils. The proposed constitutive model can simulate the mechanical behaviour of both uneroded and eroded gap-graded soils under the drained condition, which offers some important insights into the design of the earthen structures deteriorated by seepage flow. However, some limitations exist in the proposed model.

The parameter calibration was made under limited conditions (e.g., flow velocity, initial fines content, soil types) for both seepage and triaxial tests. The mechanical behaviour of the internally eroded soils is examined based only on the drained triaxial compression test after finishing the seepage test in the laboratory. However, the change in mechanical behaviour occurs during the erosion process in nature. The proposed model cannot predict the change in shearing response due to erosion during shearing, which needs further study.

Under the undrained condition, the prediction of the pore water pressure is highly related to the prediction of the volumetric strain under the drained condition. The simulated volumetric strain of the loose sand at the small strain is overestimated (Fig. 3b), in which case the simulated pore water pressure of the loose sand at the small strain under the undrained condition may also be overestimated.

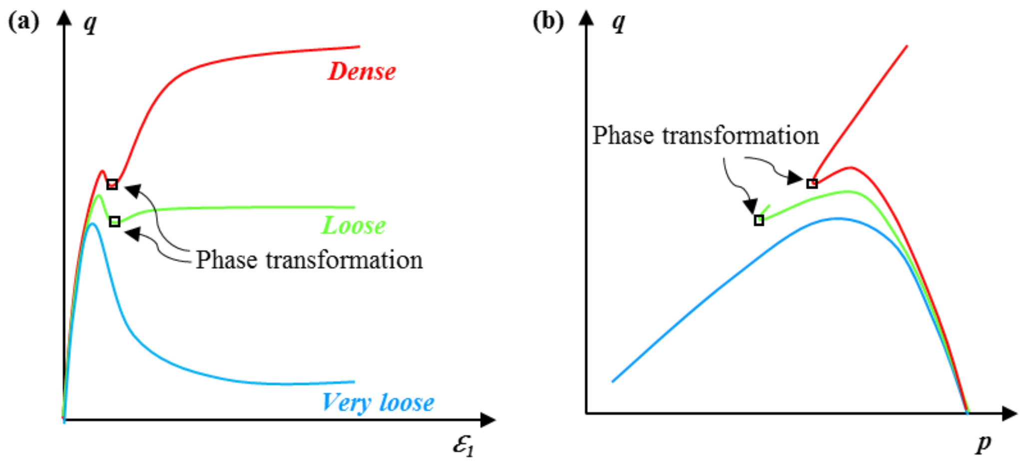

Fig. 14 Typical mechanical behaviour of sand under undrained condition and definition of phase transformation state; **(a)** deviatoric stress-axial strain response, **(b)** effective stress path

The phase transformation is a significant feature for the undrained mechanical behaviour of the soils (Fig. 14), which has also been considered in some constitutive models (Li and Dafalias, 2000; Nguyen et al., 2018, among the others). However, as the proposed constitutive model is based on the Cam-clay model, the dilative behaviour of a dense soil after passing the phase transformation point cannot be expressed.

6. Conclusions

Based on the experimental observations on the mechanical behaviour of eroded soils, the concept of the normal yield surface for the eroded soils is proposed and is implemented in the subloading Cam-clay model. The similarity ratio that characterises the size of the normal yield surface of the eroded soils to the normal yield surface of the uneroded soils is introduced to consider the change in the size of the yield surface due to erosion and its decay with the shearing.

From the experimental results and back analysis of the experimental results (Ke and Takahashi, 2014; Chen et al., 2016; Li et al., 2020), key parameters of the modified model are identified, i.e., the post-erosion void ratio, the slope of normal compression line, the angle of shearing resistance at the critical state, and the similarity ratio. The effects of the erosion on the modified model parameters are quantified. The angle of shearing resistance at the critical state has a positive linear relationship with the final fines content when the final fines content is smaller than the threshold fines content. At the same time, the slope of the normal compression line increases with the void ratio before shearing. The initial values of these key parameters can be obtained through empirical equations with curve-fitted parameters. The determination method of the erosion-related model parameters and initial conditions is proposed. The initial similarity ratio for the dense soils decreases from one with the loss of fine particles, while the initial similarity ratio for the loose soils increases slightly.

The capability of the modified subloading Cam-clay model is discussed through the simulation for the drained triaxial tests of the eroded dense soils through the laboratory tests. Comparisons between the experimental and simulation results on the eroded dense soils demonstrate the good performance of the modified model in simulating the soils subjected to erosion. By using the proposed modified model, the shearing after erosion can be simulated. However, the modified model cannot predict the change in shearing response due to erosion during shearing.

References

Al-Khafaji, A. W. N., & Andersland, O. B. (1992). Equations for compression index approximation. Journal of geotechnical engineering, 118(1), 148-153.

Andrianatrehina, N. L., Souli, H., Rech, J., Fry, J. J., Fleureau, J. M., & Taibi, S. (2016). Influence of the percentage of sand on the behavior of gap-graded cohesionless soils. Comptes Rendus Mecanique, 344(8), 539-546.

Benahmed, N., Nguyen, T. K., Hicher, P. Y., & Nicolas, M. (2015). An experimental investigation into the effects of low plastic fines content on the behaviour of sand/silt mixtures. European Journal of environmental and civil engineering, 19(1), 109-128.

Cabalar, A. F. (2011). The effects of fines on the behaviour of a sand mixture. Geotechnical and Geological Engineering, 29(1), 91-100.

Carraro, J. A. H., Prezzi, M., & Salgado, R. (2009). Shear strength and stiffness of sands containing plastic or nonplastic fines. Journal of geotechnical and geoenvironmental engineering, 135(9), 1167-1178.

Chang, C. S., & Yin, Z. Y. (2011). Micromechanical modeling for behavior of silty sand with influence of fine content. International Journal of Solids and Structures, 48(19), 2655-2667.

Chang, D. S., & Zhang, L. M. (2011). A stress-controlled erosion apparatus for studying internal erosion in soils. Geotechnical Testing Journal, 34(6), 579-589.

Chen, C., Zhang, L. M., & Chang, D. S. (2016). Stress-strain behavior of granular soils subjected to internal erosion. Journal of Geotechnical and Geoenvironmental Engineering, 142(12), 06016014.

Chen, C., Zhang, L. M., & Zhu, H. (2017). A photographic method for measuring soil deformations during internal erosion under triaxial stress conditions. Geotechnical Testing Journal, 41(1), 43-54.

Crosta, G., & Prisco, C. D. (1999). On slope instability induced by seepage erosion. Canadian Geotechnical Journal, 36(6), 1056-1073.

Fannin, R. J., & Slangen, P. (2014). On the distinct phenomena of suffusion and suffosion. Géotechnique Letters, 4(4), 289-294.

Foster, M., Fell, R., & Spannagle, M. (2000). The statistics of embankment dam failures and accidents. Canadian Geotechnical Journal, 37(5), 1000-1024.

Gai, X., & Sánchez, M. (2019). An elastoplastic mechanical constitutive model for microbially mediated cemented soils. Acta Geotechnica, 14(3), 709-726.

Habibbeygi, F., Nikraz, H., & Verheyde, F. (2017). Determination of the compression index of reconstituted clays using intrinsic concept and normalized void ratio. International Journal of GEOMATE, 13(39), 54-60.

Hashiguchi, K. (1989). Subloading surface model in unconventional plasticity. International Journal of Solids and Structures, 25(8), 917-945.

Hicher, P. Y. (2013). Modelling the impact of particle removal on granular material behaviour. Geotechnique, 63(2), 118-128.

Hosn, R. A., Sibille, L., Benahmed, N., & Chareyre, B. (2016). A discrete numerical description of the mechanical response of soils subjected to degradation by suffusion. In Scour and Erosion: Proceedings of the 8th International Conference on Scour and Erosion, September 12-15, Oxford, UK, CRC Press.

Hunter, R. P., & Bowman, E. T. (2018). Visualisation of seepage-induced suffusion and suffosion within internally erodible granular media. Géotechnique, 68(10), 918-930.

Hu, W., Hicher, P. Y., Scaringi, G., Xu, Q., Van Asch, T. W., & Wang, G. (2018). Seismic precursor to instability induced by internal erosion in loose granular slopes. Géotechnique, 68(11), 989-1001.

Hu, Z., Zhang, Y., & Yang, Z. (2020). Suffusion-Induced Evolution of Mechanical and Microstructural Properties of Gap-Graded Soils Using CFD-DEM. Journal of Geotechnical and Geoenvironmental Engineering, 146(5), 04020024.

Ke, L., & Takahashi, A. (2014). Experimental investigations on suffusion characteristics and its mechanical consequences on saturated cohesionless soil. Soils and Foundations, 54(4), 713-730.

Ke, L., & Takahashi, A. (2015). Drained monotonic responses of suffusional cohesionless soils. Journal of Geotechnical & Geoenvironmental Engineering, 141(8), 4015033.

Li, S., Russell, A. R., & Wood, D. M. (2017). Stress-strain behavior of soils having undergone different amounts of internal erosion. In Proceedings of 25th Meeting of European Working Group on Internal Erosion in Embankment Dams & their Foundations, 114-122. September 4-7, Delft, Netherlands

Li, S., Adrian Russell, David Muir Wood. (2020). The influence of particle size distribution homogeneity on the shearing of soils having been subjected to internal erosion. Canadian Geotechnical Journal, 57(11), 1684-1694.

Li, X. S., & Dafalias, Y. F. (2000). Dilatancy for cohesionless soils. Géotechnique, 50(4), 449-460.

Mahmoudi, Y., Cherif Taiba, A., Belkhatir, M., Arab, A., & Schanz, T. (2018). Laboratory study on undrained shear behaviour of overconsolidated sand–silt mixtures: effect of the fines content and stress state. International Journal of Geotechnical Engineering, 12(2), 118-132.

Mehdizadeh, A., Disfani, M. M., Evans, R., & Arulrajah, A. (2017). Progressive Internal Erosion in a Gap-Graded Internally Unstable Soil: Mechanical and Geometrical Effects. International Journal of Geomechanics, 18(3), 04017160. DOI: 10.1061/(ASCE)GM.1943-5622.0001085

Muir Wood, D., Maeda, K., & Nukudani, E. (2010). Modelling mechanical consequences of erosion. Géotechnique, 60(6), 447-457.

Nakai, T., & Hinokio, M. (2004). A simple elastoplastic model for normally and over consolidated soils with unified material parameters. Soils and foundations, 44(2), 53-70.

Nguyen, C. D., Benahmed, N., Andò, E., Sibille, L., & Philippe, P. (2019). Experimental investigation of microstructural changes in soils eroded by suffusion using X-ray tomography. Acta Geotechnica, 14(3), 749-765.

Nguyen, H. B. K., Rahman, M. M., & Fourie, A. B. (2018). Characteristic behavior of drained and undrained triaxial compression tests: DEM study. Journal of Geotechnical and Geoenvironmental Engineering, 144(9), 04018060.

Ouyang, M., & Takahashi, A. (2015). Influence of initial fines content on fabric of soils subjected to internal erosion. Canadian Geotechnical Journal, 53(2), 299-313.

Park, H. I., & Lee, S. R. (2011). Evaluation of the compression index of soils using an artificial neural network. Computers and Geotechnics, 38(4), 472-481.

Park, J. H., & Koumoto, T. (2004). New compression index equation. Journal of Geotechnical and Geoenvironmental Engineering, 130(2), 223-226.

Richards, K. S., & Reddy, K. R. (2010). True triaxial piping test apparatus for evaluation of piping potential in earth structures. Geotechnical Testing Journal, 33(1), 83-95.

Richart, F. E. Jr., Hall, J. R. & Woods, R. D. (1970). Vibrations of soils and foundations. Englewood Cliffs, NJ: Prentice-Hall.

Rousseau, Q., Sciarra, G., Gelet, R., & Marot, D. (2018,). Constitutive Modeling of a Suffusive Soil with Porosity-Dependent Plasticity. In: Bonelli S., Jommi C., Sterpi D. (eds) Internal Erosion in Earthdams, Dikes and Levees. EWG-IE 2018. Lecture Notes in Civil Engineering, 17: 168-179. Springer, Cham, Switzerland. DOI: 10.1007/978-3-319-99423-9_16

Rousseau, Q., Sciarra, G., Gelet, R., & Marot, D. (2020). Modelling the poroelastoplastic behaviour of soils subjected to internal erosion by suffusion. International Journal for Numerical and Analytical Methods in Geomechanics, 44(1): 11-136, DOI: https://doi.org/10.1002/nag.3014

Salgado, R., Bandini, P., & Karim, A. (2000). Shear strength and stiffness of silty sand. Journal of Geotechnical and Geoenvironmental Engineering, 126(5), 451-462.

Seed, B., & Lee, K. L. (1966). Liquefaction of saturated sands during cyclic loading. Journal of Soil Mechanics & Foundations Div, 92(6): 105-134.

Shibata, T. (1963). On the volume changes of normally consolidated clays. Annuals, Disaster Prevention Research Institute, Kyoto University, 6, 128-134. (in Japanese)

Tiwari, B., & Ajmera, B. (2012). New correlation equations for compression index of remolded clays. Journal of Geotechnical and Geoenvironmental Engineering, 138(6), 757-762.

Wang, G., Horikoshi, K., & Takahashi, A. (2020). Effects of Internal Erosion on Parameters of Subloading Cam-Clay Model. Geotechnical and Geological Engineering, 38(2), 1323-1335.

Wang, X., & Li, J. (2015). On the degradation of granular materials due to internal erosion. Acta Mechanica Sinica, 31(5), 685-697.

Wichtmann, T., Hernández, M. N., & Triantafyllidis, T. (2015). On the influence of a non-cohesive fines content on small strain stiffness, modulus degradation and damping of quartz sand. Soil Dynamics and Earthquake Engineering, 69, 103-114.

Wilson, G. V., Wells, R., Kuhnle, R., Fox, G., & Nieber, J. (2018). Sediment detachment and transport processes associated with internal erosion of soil pipes. Earth Surface Processes and Landforms, 43(1), 45-63.

Xiao, M., & Shwiyhat, N. (2012). Experimental investigation of the effects of suffusion on physical and geomechanic characteristics of sandy soils. Geotechnical Testing Journal, 35(6), 890-900.

Xiao, Y., Xiang, J., Liu, H., & Ma, Q. (2017). Strength–dilatancy relation of sand containing non-plastic fines. Géotechnique Letters, 7(2), 204-210.

Yang, J., Yin, Z., Laouafa, F., & Hicher, P. (2019). Internal erosion in dike - on - foundation modeled by a coupled hydromechanical approach. International Journal for Numerical and Analytical Methods in Geomechanics, 43(3), 663-683.

Yang, J., Yin, Z., Laouafa, F., & Hicher, P. (2020). Hydromechanical modeling of granular soils considering internal erosion. Canadian Geotechnical Journal, 57(2), 157-172.

Zhang, F., Li, M., Peng, M., Chen, C., & Zhang, L. (2019). Three-dimensional DEM modeling of the stress–strain behavior for the gap-graded soils subjected to internal erosion. Acta Geotechnica, 14(2), 487-503.

Zhang, S., Leng, W., Zhang, F., & Xiong, Y. (2012). A simple thermo-elastoplastic model for geomaterials. International Journal of Plasticity, 34, 93-113.

Zhang, Y., & Chen, Y. (2017). A constitutive relationship for gravelly soil considering fine particle suffusion. Materials, 10(10), 1217.

Zhuang, J., Peng, J., Zhu, Y., Leng, Y., Zhu, X., & Huang, W. (2021). The internal erosion process and effects of undisturbed loess due to water infiltration. Landslides, 18, 629–638.

Zuo, L. & Baudet, B. A. (2015). Determination of the transitional fines content of sand-non plastic fines mixtures. Soils and Foundations, 55(1), 213-219.